

Influence of vitamin D receptor signaling and vitamin D on colonic epithelial cell fate decisions in ulcerative colitis

Lauge Kellermann¹, Stine Lind Hansen², Grzegorz Maciag², Agnete Marie Granau¹, Jens Vilstrup Johansen³, Joji Marie Teves^{2,3}, Raul Bardini Bressan², Marianne Terndrup Pedersen³, Christoffer Soendergaard¹, Astrid Moeller Baattrup², Alexander Hammerhøj¹, Lene Buhl Riis⁴, John Gubatan⁵, Kim Bak Jensen^{2*}, Ole Haagen Nielsen^{1*}

¹Department of Gastroenterology, Herlev Hospital, Faculty of Health and Medical Sciences, +University of Copenhagen, DK-2730 Herlev, Denmark

²Novo Nordisk Foundation Center for Stem Cell Medicine (reNEW), Faculty of Health and Medical Sciences, University of Copenhagen, DK-2200 Copenhagen N, Denmark

³Biotech Research and Innovation Centre, University of Copenhagen, DK-2200 Copenhagen N, Denmark

⁴Department of Pathology, Herlev Hospital, University of Copenhagen, DK-2730 Herlev, Denmark

⁵Division of Gastroenterology and Hepatology, Stanford University School of Medicine, Stanford, 94305 CA, USA

*Corresponding authors

Ole Haagen Nielsen, Department of Gastroenterology D112, Borgmester Ib Juuls Vej 1, DK-2730 Herlev, Denmark, Phone +45 38689522, Email: ole.haagen.nielsen@regionh.dk

Kim B. Jensen, Novo Nordisk Foundation Center for Stem Cell Medicine (reNEW), Blegdamsvej 3B, DK-2200 Copenhagen N, Denmark, Phone +45 35325682, Email: kim.jensen@sund.ku.dk

Conference presentation

Data from this study was presented in part at the American College of Gastroenterology Annual

Meeting, Vancouver, BC, October 20-25, 2023.

© The Author(s) 2024. Published by Oxford University Press on behalf of European Crohn's and Colitis Organisation.

This is an Open Access article distributed under the terms of the Creative Commons Attribution-NonCommercial License (<https://creativecommons.org/licenses/by-nc/4.0/>), which permits non-commercial re-use, distribution, and reproduction in any medium, provided the original work is properly cited. For commercial re-use, please contact journals.permissions@oup.com

Abstract

Background and aims: Epidemiological studies have shown that subnormal levels of vitamin D (25(OH)D) are associated with a more aggravated clinical course of ulcerative colitis (UC). Despite an increased focus on the therapeutic importance of vitamin D and vitamin D receptor (VDR) signaling, the mechanisms underlying the effects of the vitamin D–VDR axis on UC remain elusive. Therefore, we aimed to investigate whether exposure to active vitamin D (1,25(OH)₂D₃)/VDR signaling in human organoids could influence the maintenance of the colonic epithelium.

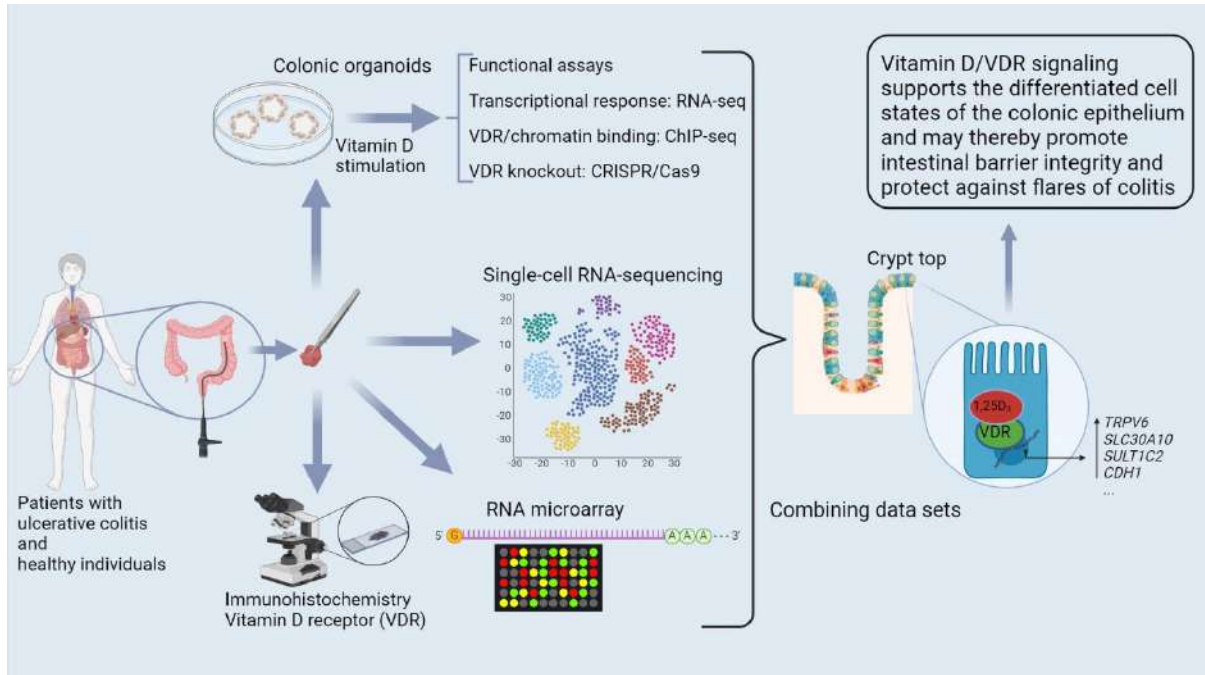
Methods: Intestinal VDR expression was studied by immunohistochemistry, RNA expression arrays, and single-cell RNA sequencing of colonic biopsy specimens obtained from patients with UC and healthy individuals. To characterize the functional and transcriptional effects of 1,25(OH)₂D₃, we used patient-derived colonic organoids. The dependency of VDR was assessed by knocking out the receptor with CRISPR/Cas9.

Results: Our results suggest that 1,25(OH)₂D₃/VDR stimulation supports differentiation of the colonic epithelium and that impaired 1,25(OH)₂D₃/VDR signaling thereby may compromise the structure of the intestinal epithelial barrier, leading to flares of UC. Furthermore, a transcriptional response to VDR activity was observed primarily in fully differentiated cells at the top of the colonic crypt, and this response was reduced during flares of UC.

Conclusions: We identified an important role of vitamin D signaling in supporting differentiated cell states in the human colonic epithelium, and thereby maintenance of the intestinal barrier integrity. This makes the vitamin D–VDR signaling axis an interesting target for therapeutic efforts to achieve and maintain remission in patients with UC.

Keywords: Colonic epithelium; inflammatory bowel disease; vitamin D.

Graphical abstract



Accepted Manuscript

Introduction

The global burden of ulcerative colitis (UC), the most prevalent form of inflammatory bowel disease (IBD), is increasing.^{1,2} Today, more than 1 million patients diagnosed with UC are living in North America,³ and more than 1.5 million in Europe.⁴ The inflammation in UC affects the epithelial lining of the colon and rectum, with relapsing symptomatic periods alternating with disease-free (quiescent) intervals.⁵ UC is a multifactorial disease,⁶ and flares of UC are a major cause of debilitating symptoms among affected individuals as well as a significant socioeconomic burden for the society.⁷ In recent years, a variety of treatment options, including biologics and small molecules, have emerged⁸⁻¹⁰; however, there is still room for improvement in UC care and a further need for relevant models with which to study its pathology.¹¹ Colonic organoids have recently proven a robust system for studying the pathophysiology of intestinal epithelial cells (IECs) at the molecular level.^{6,12}

In large epidemiological studies, subnormal levels of vitamin D (25(OH)D) in the serum have been linked to adverse clinical outcomes in patients with ulcerative colitis (UC).¹³⁻²⁰ Vitamin D insufficiency (i.e., serum 25(OH)D level \leq 50 nmol/l (20 ng/l)), affects skeletal health, although the optimal levels for extra-skeletal health may be higher.^{21,22} However, the clinical benefits of vitamin D supplementation in patients with IBD, as well as the link between vitamin D status and IBD, remain unclear.^{23,24}

Vitamin D signaling is active in the colonic epithelium, which constitutes the intestinal barrier that faces the gut lumen.²⁵ The hormonal active form of vitamin D, calcitriol ($1\alpha,25$ -dihydroxyvitamin D₃ (1,25(OH)₂D₃)), is a pleiotropic hormone produced by the enzymatic hydroxylation of 25(OH)D₃ by CYP27B1 in the kidney and in target tissues, such as the intestine.²⁶ In cells, 1,25(OH)₂D₃ binds to vitamin D receptor (VDR), which facilitates heterodimerization of VDR with the retinoid X receptor. This heterodimer subsequently binds to DR3-type vitamin D response elements (VDREs) in the genome and regulates the transcription of target genes.²⁷ While normal VDR expression levels seem

to be correlated with a reduced risk of developing UC and a better response to treatment,²⁸ the functional role of VDR has yet to be fully described. Nonetheless, several studies investigating VDR function in experimental animal models have revealed that 1,25(OH)₂D₃/VDR signaling plays an important role in mitigating the severity of chemically induced experimental colitis.²⁹⁻³⁸ This activity is connected to a plethora of different mechanisms, including modification of immune cell functions, intestinal barrier integrity, autophagy, Paneth cell function, and crosstalk with the gut microbiome.²⁹⁻³⁸ While VDR signaling clearly plays an important role in the colonic epithelium, a need to further elucidate its specific functions remains, and more importantly, how these studies translate to the human epithelium, and the potential role of 1,25(OH)₂D₃/VDR signaling in UC, remain unknown.

We hypothesized that 1,25(OH)₂D₃ plays a role in the maintenance of the intestinal epithelial barrier and may be able to directly affect IECs and mechanisms related to intestinal homeostasis. Based on this hypothesis, we aimed to investigate whether 1,25(OH)₂D₃ exposure and VDR signaling in human IECs might play an active role in UC. To this end, we exploited colonic organoids derived from patients with UC and healthy controls to test the effects of these substances on stem cell properties and differentiation. This approach was combined with an analysis of patient biopsy samples to define VDR expression and to identify specific subtypes of IECs with VDR transcriptional activity, in an effort to determine the clinical relevance of VDR. We revealed that 1,25(OH)₂D₃ exposure restricts organoid growth and drive the intestinal epithelial cells towards a more differentiated state in a VDR-dependent manner. Moreover, by investigating VDR transcriptional activity via single-cell RNA sequencing (scRNA-seq) analyses, we showed that VDR is expressed in the colonic epithelium, primarily at the crypt-top, and that VDR expression inversely correlates with disease severity and inflammation status in patients with UC. Thus, the present study provides novel insights into how subnormal levels of vitamin D and VDR signaling may influence the clinical course of UC.

MATERIALS AND METHODS

Study population and approval

The individuals included in this study were all scheduled for a lower endoscopy at the Department of Gastroenterology, Herlev Hospital, University of Copenhagen, Denmark, due to various clinical conditions. All patients with UC were diagnosed based on well-established criteria.⁵ Healthy individuals were identified from the Danish National Screening Program for Colorectal Cancer or evaluated for various gastrointestinal symptoms but were included only if all subsequent examinations were normal. The exclusion criteria included age below 18 or over 80 years; clinical evidence of infection; use of antibiotics within 14 days of the study; severe mental illness; and pregnancy/lactation. Information regarding sex, age, medical history, and medication history were collected from each individual. No predefined matching between groups of UC and healthy individuals was performed. This study was approved by the Scientific Ethics Committee of the Capital Region of Denmark (reg. no. H-18005342). All individuals were informed of the study both orally and in writing, in compliance with the Declaration of Helsinki and the guidelines of the Danish National Scientific Ethics Committee. Written informed consent was obtained prior to inclusion.

Gene expression dataset, histologic specimens, and blood sample analysis

Transcriptomic data from a previously described patient cohort at Herlev Hospital (available at NCBI GEO GSE206171), which included healthy individuals and patients with UC, were used to analyze *VDR* gene expression and the identified *VDR* target genes (Supplementary Table S1).³⁹⁻⁴¹ Disease activity was assessed by the Mayo score, which evaluates four clinical parameters, namely, stool frequency, rectal bleeding, endoscopic findings, and the physician's global assessment, and assigns a score of 0, 1, 2, or 3 for each parameter to generate a total score between 0 and 12.⁴² A total score of 0–2 indicates remission or quiescent disease, 3–5 indicates mild disease, 6–10 indicates moderate disease, and 11–12 indicates severe disease. Four sigmoid colon biopsy samples were collected from each individual. RNA was obtained from two biopsy samples and analyzed by microarray using the 3-

IVT expression kit and HGU219 chip (Affymetrix, Santa Clara, CA, USA) as previously described.⁴⁰ Two additional biopsy samples were fixed in formalin for histological examination, and blood samples were analyzed with Luminex xMAP Technology as previously described.⁴¹ Blood samples collected at time of endoscopy were analyzed for serum 25(OH)D levels using a Vitamin D Total Immunoassay on an Atellica IM analyzer at the Department of Clinical Biochemistry, Herlev Hospital, Denmark.

Single-cell RNA sequencing dataset

We analyzed our recent scRNA-seq dataset of sigmoid colonic biopsy specimens collected from four healthy individuals and four patients experiencing UC flares. Epithelial cells were mechanically and enzymatically released from the colonic crypts as described below and isolated by flow cytometric sorting for cells that were positive for the epithelial cell marker EpCAM. The single-cell suspension was further processed on the 10X Genomics platform for scRNA-seq analysis, as described by Maciag et al.⁴³

Establishment of organoid cultures

Sigmoid colon biopsies for the organoid cultures were obtained from six healthy individuals and six patients with UC. The characteristics of the patients are shown in Supplementary Table S2. The employed protocol was based on that described by Sato et al.,⁴⁴ with slight modifications as previously described.⁴⁵ Details on organoid experiments may be found in the Supplementary Materials.

1,25(OH)₂D₃ stimulation of organoids

Intestinal organoid (IO)-medium (Supplementary Table S3) was supplemented with 1,25(OH)₂D₃ (cat. no. 71820, Cayman Chemical, Ann Arbor, MI, USA) or ethanol as a vehicle control. All experiments were performed in triplicate. For continuous stimulation in the proliferation assay, a final concentration of 100 nM 1,25(OH)₂D₃/ethanol (0.01%) was used. For short-term stimulation at 2, 6, and 24 h, a concentration of 1 μM 1,25(OH)₂D₃/ethanol (0.1%) was used to strengthen chromatin

binding and the transcriptional response. For stimulation experiments, fresh medium was prepared each time by diluting a $1,25(\text{OH})_2\text{D}_3$ (1 mM) stock solution to the desired concentration in IO-medium immediately prior to use.

Histological scoring and VDR staining intensity scoring

Slides with two formalin-fixed and paraffin-embedded sigmoid colon biopsy specimens from each individual in the previously described cohort were stained with hematoxylin and eosin and the D2K6W anti-VDR antibody as described in Supplementary Methods.⁴¹ The slides were assessed by a pathologist specializing in gastroenterology who was blinded to patient information. Based on the overall VDR expression in each of the two biopsy specimens, an immunohistochemical staining intensity score of 0, 1, 2, or 3 (Supplementary Figure S1A-B) was assigned, and the mean score for each patient was used for further analyses. Histological inflammatory activity was graded according to the Geboes score,⁴⁶ in which a score was assigned to each of the following six histopathological parameters: architectural changes, chronic inflammatory infiltrate, lamina propria neutrophils and eosinophils, epithelial neutrophils, crypt destruction, and ulceration. For statistical analysis, the sum of the subscores on a scale of 0–22 was used. To demonstrate VDR expression in the full colonic crypt axis, sections of normal sigmoid colon from surgical colorectal cancer resection specimens and colonic resection specimens from patients with ulcerative colitis were included (n=5). Detailed information on immunohistochemistry (IHC), may be found in the Supplementary Materials.

RNA and protein analysis of intestinal organoids

RNA and protein were extracted from intestinal organoids using NucleoSpin columns (Macherey-Nagel, Duren, Germany) according to the manufacturer's instructions. The RNA concentration was determined using a NanoDrop One spectrophotometer (Thermo Fischer Scientific). Detailed information on western blotting and qPCR may be found in the Supplementary Materials.

RNA sequencing

Organoids from one healthy individual were used to study the transcriptional response to 1,25(OH)₂D₃ or vehicle after 6 and 24 h of exposure on day 6 after passage using total RNA-seq (the data are available at NCBI GEO GSE206176). The RNA integrity number (RIN) was measured using a Bioanalyzer 2100 with an Agilent RNA 6000 Nano Kit. All RIN values were >9.7 (threshold for inclusion was >8.0). For library preparation, 500 ng of each sample was processed with a TruSeq RNA Sample Prep Kit v2 (Illumina, San Diego, CA, USA), and the samples were sequenced using the Illumina Next-Seq 500 platform in accordance with the manufacturer's instructions.

RNA-seq data analysis

The quality of the raw 76 bp single-end sequence RNA-seq reads was evaluated using FastQC⁴⁷ and FastQ Screen⁴⁸. Raw reads were trimmed with FastQ preprocessor (v0.21.0)⁴⁹ using the default settings ('--trim_poly_g --trim_poly_x --cut_tail --trim_front1 12 --trim_tail1'). The trimmed mRNA-seq reads were aligned to the human genome (hg38 assembly) using STAR aligner⁵⁰ (v2.6.0c) in two-pass mode and guided by a RefSeq (UCSC) gene annotation (default settings except --sjdbOverhang 62 --twopassMode Basic --outSAMtype BAM SortedByCoordinate --outSAMattributes All --outSAMunmapped Within --outFilterMismatchNoverLmax 0.1 --outFilterMatchNmin 25 --outFilterMismatchNmax 10).

After mapping, the reads were assigned to genes with featureCounts⁵¹ (v1.5.1, settings: -s 0 -J), and a count table was generated. The DESeq2⁵² (v1.22.1) package in R (v3.5.1), was used for statistical analysis of the count data from the different groups. Gene Ontology (GO) analysis was performed using the R package gprofiler2. Selected GO terms were chosen based on their adjusted p-values ($p < 0.05$) and biological relevance. The query-gene lists used up- and downregulated genes based on the RNAseq analysis of differentially expressed genes between 1,25(OH)₂D₃ stimulated or unstimulated cultures.

ChIP-seq

Organoids established from one healthy individual were used for ChIP-seq experiments (data available at NCBI GEO GSE206177). The healthy individual was a middle aged (54 y) female without intestinal disease and was chosen as a representative of the normal colonic epithelium. On day 6, the organoids were stimulated with $1,25(\text{OH})_2\text{D}_3$ (1 μM) or the vehicle for 2 h. In this study, 90 Matrigel droplets were used for each condition to obtain enough chromatin for the analysis. The organoids were collected, and the pellet was resuspended and incubated in 3 ml of Cell Recovery Solution (Corning) for 25 min on ice, centrifuged at $300 \times g$ for 3 min, and washed 3 times in PBS with 0.1% BSA. The cells were then fixed for 10 min in methanol-free formaldehyde (1%), and chromatin was prepared for shearing with a Covaris M-220 sonicator using a truChIP Chromatin Shearing Kit (Covaris, Woburn, MA, USA) in accordance with the manufacturer's instructions. Sheared product size was controlled using the truChIP kit. DNA was purified using a MinElute PCR purification kit (Qiagen, Hilden, Germany), and fragment sizes were measured with a 2100 Bioanalyzer High Sensitivity DNA Kit (Agilent Technologies). Chromatin shearing was continued until a product size of 150–300 bp was reached. The DNA concentration was determined using an Invitrogen Qubit 4 fluorometer (Invitrogen).

A total of 11 μg of chromatin from each $1,25(\text{OH})_2\text{D}_3$ - and vehicle-stimulated sample was diluted 1:1 in immunoprecipitation (IP) buffer (truChIP Kit, Covaris) for a total volume of 550 μl . The samples were precleared using 20 μl of Magnetic Protein A Dynabeads (Invitrogen) for 1 h with rotation at 4 $^\circ\text{C}$. Next, 5 μl of the sample was stored as a 1% input control, and 500 μl (10 μg of chromatin) was prepared for IP with 10 μl of a rabbit IgG anti-VDR antibody (D2K6W, Cell Signaling) and incubated overnight at 4 $^\circ\text{C}$ with rotation. Immunocomplexes were captured using magnetic beads for 2 h at 4 $^\circ\text{C}$ with rotation, and the beads were collected with a magnetic rack. The magnetic beads were then washed for 5 min with rotation in each of the following buffers: three washes with a 150 mM Wash Buffer (low salt), three washes with a 500 mM Wash Buffer (high salt), one wash with LiCl buffer,

and one wash with TE buffer. All buffers were from the ChIP-Assay Kit (17-295, Millipore, Sigma–Aldrich).

The magnetic beads and input controls were diluted to 90 μ l in TE buffer supplemented with RNase (50 μ g/ml, Thermo Fisher Scientific), Proteinase K (0.5 mg/ml, Thermo Fisher Scientific), and SDS (Invitrogen), yielding a final concentration of 0.5%, and incubated at 65 °C overnight to de-crosslink the DNA complexes. DNA was purified using a Qiagen MinElute PCR purification kit.

Library preparation and sequencing: Purified DNA was quantified using a Qubit fluorimeter, and 20 ng was used as the input material. ChIP-seq libraries were prepared with an NEBNext Ultra II DNA Library Kit (cat. no. E7103) and NEBNext multiplex oligos for Illumina (cat. no. E7335 and E7600), following the manufacturer's instructions. The concentration of each library was measured using a Qubit, and size distributions were estimated using a D1000 ScreenTape assay (Agilent Technologies). Libraries were pooled at an equimolar ratio based on the concentration and size distribution values of the individual libraries. The library pool was then diluted and processed for sequencing using the Illumina Next-Seq 500 platform in accordance with the manufacturer's instructions.

ChIP-seq data analysis

The quality of the raw 75 bp single-end sequence reads was evaluated using FastQC⁴⁷ and FASTQ Screen⁴⁸. Raw reads were trimmed with FastQ preprocessor⁴⁹ (v0.21.0) using the default settings ('-trim_poly_g --trim_poly_x --cut_tail --trim_front1 1'). Reads were mapped to the human genome (hg38 assembly) with Bowtie⁵³ (v1.1.2) with the default settings, except m=1 (suppress all alignments if >1 exist), -S (write output in SAM format), and excluding all haplotype variants and random and unknown chromosomal sequences (i.e., canonical chromosome sequences only). The alignment files were sorted and indexed with SAMtools (v1.10). Chromosome positions were annotated according to the RefSeq database using the UCSC 'ncbiRefSeqCurated' tables (downloaded Oct 29th, 2019). The

RefSeq annotation contained 65 484 unique transcripts, corresponding to 27 995 unique genes. The mean fragment length was estimated using the SPP peak caller function 'run_spp'.⁵⁴

Peak calling was performed using MACS2⁵⁵ (v2.1.1.20160309) in two steps: first, calling peaks against each sample's own input control using 'macs2 callpeak' with the size estimates from SPP, and second, calling differentially enriched peaks in contrast to other samples using 'macs2 bdgdiff' with the effective depth estimates from the first step. The genomic sequences inside the MACS2-called differentially enriched peaks from 'bdgdiff' were searched for motif enrichment using the webtool MEME-CHIP⁵⁶ ('meme./seqs-centered -oc meme_out -mod zoops -nmotifs 3 -minw 6 -maxw 15 -bfile./background -dna -searchsize 100000 -time 2919 -revcomp -nostatus'). The UCSC Genome Browser was used to produce tracks showing ChIP-seq enrichment and MACS2-called peaks across specific genes. The 'deeptools' package (v3.2.1) was used to make heatmaps showing the ChIP-seq signal across peaks based on normalized read density bigWig files.

A read density bigWig file was produced for each sample by normalization against its respective input control using 'bamCompare' (default settings except --binSize 50 --extendReads 250 --scaleFactorsMethod SES --ignoreForNormalization chrM). Next, the read density was extracted for each differentially enriched peak set +/-10 kb using 'computeMatrix reference-point' (default settings except '-a 10 000 -b 10 000 --skipZeros'), and the data were ultimately plotted with 'plotHeatmap'.

The two differentially enriched peak sets were merged into a single peak set (253 peaks), and determination overlap with gene annotations was performed with the 'read_distribution.py' tool from the RSEQC package.⁵⁷

To further illustrate the enrichment of VDR-binding sites in the merged peak set compared to those in the genomic background, binding site predictions for two VDR motifs from the JASPAR motif database were downloaded

(http://expdata.cmmt.ubc.ca/JASPAR/downloads/UCSC_tracks/2020/hg38/); the overlap was

determined with 1 kb genomic nonoverlapping bins. The number of VDR-binding site predictions per bin was calculated, summarized, and plotted. The correlation between the predicted VDR-binding sites and gene expression was illustrated through a GSEA plot based on the merged peak set and the log₂ fold change gene expression at 6 h for 1,25(OH)₂D₃ vs. vehicle using the R package 'fgsea' (v1.16.0). Unless otherwise stated, all RNA-seq and ChIP-seq plots were generated in R (v.4.0.3) with either base plotting functions or the 'ggplot2' R package.

CRISPR/Cas9 knockout of VDR

To determine whether the effects of 1,25(OH)₂D₃ are mediated directly by VDR, the receptor-encoding gene was knocked out using CRISPR/Cas9 in organoids from a healthy individual. A commercially available CRISPR Knockout All-In-One construct (Applied Biological Materials, Richmond, BC, Canada) consisting of three nonviral vectors was applied. Nucleofection was performed with a NEPA21 electroporator (Nepa Gene Co., Chiba, Japan) according to a protocol from Fujii et al.,⁵⁸ with slight modifications.

For each electroporation, 10 wells of organoids seeded at 7 500 cells per Matrigel droplet were used. On day 2, the medium was changed to IO-medium without antibiotics, Wnt3A or R-spondin1 but supplemented with CHIR99021 (5 μM, Calbiochem) and Y-27632 (10 μM). On day 3, 1.25% (vol/vol) DMSO was added to the medium. On day 4, the organoids were collected and dissociated into smaller clusters of 3–6 cells by incubation with TrypLE for 10 min at 37 °C followed by pipetting with a P1000 pipet. The cells were then washed twice in Opti-MEM (Thermo Fisher Scientific) and centrifuged at 500 ×g for 5 min. For each electroporation, the cells were resuspended in 100 μl of Opti-MEM including either 15 μg of CRISPR/Cas9 plasmid DNA (5 μg of each of the three plasmids) or 15 μg of GFP plasmid as a transfection control.

Cell suspensions were transferred to Nepa electroporation cuvettes, which were treated using a NEPA21 electroporator with the settings presented in Supplementary Table S4. After electroporation, 400 μ l of Opti-MEM + Y-27632 (10 μ M) was added to the cuvette, and the cells were incubated at ambient temperature for 30 min. The cells were then transferred to a 15 ml tube with advanced DMEM-F12 medium and centrifuged at 500 $\times g$ for 5 min. The cells were seeded in six Matrigel droplets in IO-medium without antibiotics, Wnt3A or R-spondin1 but supplemented with CHIR99021 (5 μ M), Y-27632 (10 μ M) and DMSO (1.25% vol/vol). On day 1 after transfection, DMSO was removed from the medium, and on day 3, the medium was replaced with normal IO-medium. To select for *VDR* knockout cells, 1,25(OH)₂D₃ (1 μ M) was added to the medium on day 3, and the cells were cultured for 8 passages with continued 1,25(OH)₂D₃ stimulation. Sanger sequencing analysis confirmed the presence of several frame-shift mutations in the *VDR* gene product in the *VDR*-knockout organoid culture, and Western blotting confirmed *VDR* knockout at the protein level.

PCR and Sanger sequencing of CRISPR/Cas9-edited samples

The *VDR* cDNA gene product from three replicates of *VDR* knockout cells and parental cells was amplified by PCR (forward primer 5'-3': GCACTTCCTGCCTGACC and reverse primer 5'-3': GTACGTCTGCAGTGTGTTGG). The PCR products were analyzed on a 2% agarose gel. PCR products were purified using a Qiagen MinElute kit and subsequently submitted for Sanger sequencing at Eurofins Genomics. CRISPR editing data were analyzed with Synthego's free online ICE CRISPR editing tool.⁵⁹

Statistical analysis

RNA-seq and ChIP-seq data were analyzed as described above. The scRNA-seq data were analyzed using previously described methods.⁴³ Statistical analysis of the experimental data was performed using R and GraphPad Prism 9. Gene expression levels between groups from the RNA array assay were analyzed by one-way ANOVA with Tukey's multiple comparison test. The correlation between gene expression levels and disease activity was analyzed by Spearman correlation test. Comparisons

of data between groups of organoids stimulated with $1,25(\text{OH})_2\text{D}_3$ or the vehicle control were done by the Wilcoxon test, Welch test, and Mann–Whitney U test. The Wilcoxon test was used to compare percentages of cell types in the scRNA-seq data sets. *P* values < 0.05 were considered to indicate statistical significance.

Results

Colonic VDR expression is reduced in patients with active UC and is not correlated with circulating 25(OH)D levels

To characterize vitamin D signaling in the colonic epithelium, we first aimed to determine VDR expression in sigmoid colonic biopsy specimens from a previously described patient cohort of 59 patients with UC and 19 healthy individuals (Supplementary Table S1).^{39–41} VDR expression was evaluated at the RNA level using expression arrays (Figure 1A), and at the protein level with immunohistochemistry (Figure 1B–E). To correlate VDR expression to disease severity, the patients were stratified by the Mayo score and the Geboes score.⁴² According to both methods, the VDR levels were clearly reduced in patients with active disease compared to healthy individuals and patients with quiescent disease ($P < 0.0001$) (Figure 1F–G). To investigate whether VDR expression was related to vitamin D availability, we measured serum levels of 25(OH)D and vitamin D-binding protein, the main carrier of vitamin D metabolites in the blood, in the patient cohort. There was, however, no correlation between VDR expression and 25(OH)D levels, and no significant differences in the mean serum levels of 25(OH)D or vitamin D-binding protein between healthy individuals and patients with UC in this cohort (Supplementary Figure S1C–E). Thus, a clear inverse correlation between VDR expression levels and disease severity in patients suffering from UC was observed, whereas serum levels of 25(OH)D did not correlate significantly with disease severity.

Colonic VDR expression is high in crypt-top epithelial cells

To further understand the role of VDR, we characterized colonic *VDR* expression at the single-cell level to determine where in the colonic epithelium *VDR* is expressed and investigate differences in cell population composition between UC and healthy tissue. To this end, we analyzed a newly generated scRNA-seq dataset of colonic epithelial cells isolated from four healthy individuals and four patients with active UC.⁴³ The patients all had sigmoid involvement only and mild to moderate disease activity (endoscopic Mayo score of I–II). Biopsies were obtained from visually inflamed areas and from the normal sigmoid colon in healthy individuals. In total, 11 035 epithelial cells from healthy colons were analyzed. The epithelial cells could be sorted into 13 distinct clusters, including stem cells, distinct populations of transit amplifying cells, goblet cells, enteroendocrine cells, tuft cells, and two types of colonocytes (Figure 2A). The identities of the cell clusters were based on expression of cell type specific markers as described.⁴³ *VDR* expression was detected in all epithelial cell subtypes, whereas high levels were noted in the fully differentiated crypt-top colonocyte populations (Figure 2B). Immunohistochemical analysis confirmed that *VDR* was detected along the entire crypt in the normal colon, with high expression levels in the crypt-top domain that faces the lumen (Figure 2E, top panels).

Analysis of scRNA-seq data from 4 354 cells from UC samples revealed *VDR* expression in the same 13 distinct cell clusters as seen in the healthy tissues (Figure 2C-D). We have previously shown that the cellular composition of the intestinal epithelium is altered during inflammation, with an increased stem cell fraction in inflamed UC samples.⁴³ Here, we found that the fraction of crypt-top cells in UC samples was lower than that in healthy samples, although not significantly so (Figure 2F; $P = 0.057$). To further support this finding we analyzed the RNA array dataset for expression levels of the top 20 genes defining the crypt-top colonocyte population in the scRNAseq analysis. The expression levels of 15 of these genes were inversely correlated with disease activity assessed by the Mayo score,⁴² four genes showed no significant correlation, and only one gene were positively

correlated with disease activity (Table 1). This observation reveals a lower expression of crypt-top marker genes in the inflamed UC samples across cohorts, which aligns with the observation that epithelial cells are lost or damaged, e.g., due to erosion and ulceration in the inflamed intestinal areas of UC. At the tissue level, the loss of a well-defined crypt-top layer was observed in ulcerated samples as compared to healthy tissue samples (Figure 2E). This observation nicely reflects the altered cell composition in the inflamed samples seen in the single-cell data set. Accordingly, in active UC, changes in the cellular composition of the colonic epithelium are seen as a decrease in the number of transcriptionally defined crypt-top cells and a loss of a well-defined crypt-top layer due to ulceration observed in the histological samples. This decrease appears to be associated with a decrease in *VDR* expression, as observed in both the RNA-array analysis and the histological staining, indicating that *VDR* expression is present primarily in the crypt-top layer.

1,25(OH)₂D₃ restricts the formation capacity and growth of human colonic organoid cultures

To further elucidate the importance of *VDR* signaling in the intestinal epithelium and in UC, we investigated the direct effects of 1,25(OH)₂D₃ on IECs by establishing intestinal organoids from sigmoid colon samples from six healthy individuals and six patients with quiescent UC. To determine differences between groups, organoid growth, formation and viability were considered as phenotypes when characterizing the IECs. Samples from patients with quiescent UC were chosen to avoid potential transient effects of active inflammation on organoids immediately after establishment.⁶⁰ Patient characteristics are shown in Supplementary Table S2.

VDR was found to be expressed in the established organoids (Figure 3A). Despite slight inter-individual variations in organoid morphology and growth, there were no substantial morphological differences between organoids from healthy individuals and those from patients with UC (Figure 3B). The organoids grown in cell culture medium containing 1,25(OH)₂D₃ (100 nM) for 10 days showed a significant smaller organoid size, lower numbers of formed organoids, and a lower cell yield per

seeded cell than cultures grown in medium containing the vehicle control (Figure 3B–D, Supplementary Figure S2A). Regardless of the phenotype examined, exposure to $1,25(\text{OH})_2\text{D}_3$ triggered a similar response in organoids derived from healthy individuals and UC patients (Supplementary Figure S2B, Figure 3B).

To further assess the effects of $1,25(\text{OH})_2\text{D}_3$ on the self-renewal capacity, we performed organoid formation assays starting from single cells. After treatment with $1,25(\text{OH})_2\text{D}_3$ or with ethanol as the vehicle control for 10 days, the organoids were dissociated into single cells, replated and subsequently maintained in control medium for another 10 days. Organoid formation capacity was defined as the fraction of cells that retained the ability to form an organoid. The organoid formation capacity was significantly reduced after $1,25(\text{OH})_2\text{D}_3$ stimulation, demonstrating that $1,25(\text{OH})_2\text{D}_3$ reduced the fraction of cells with self-renewal potential (Figure 3E–F). As discussed below this might be due to the induction of a more differentiated cell state by $1,25(\text{OH})_2\text{D}_3$ /VDR signaling in the organoid model. However, this effect did not differ between organoids derived from patients with quiescent UC and healthy controls, suggesting that patients with UC do not have an altered responsiveness to vitamin D signaling *per se*.

The effect of $1,25(\text{OH})_2\text{D}_3$ on colonic organoid growth and self-renewal is directly mediated by VDR

To assess whether the inhibitory effects of $1,25(\text{OH})_2\text{D}_3$ on organoid growth were mediated by VDR, we used CRISPR/Cas9 technology to genetically knock out *VDR* in an organoid culture derived from a healthy individual (Figure 4A and Supplementary Figure S3A–D). Following deletion of *VDR*, the organoids became resistant to the effects of $1,25(\text{OH})_2\text{D}_3$ on the cell yield per seeded cell, organoid size, number of organoids, and organoid formation capacity and could even be cultured extensively in the presence of $1,25(\text{OH})_2\text{D}_3$ (Figure 4B–F). These observations demonstrate that $1,25(\text{OH})_2\text{D}_3$ impacts the functions of the intestinal epithelial cells in a VDR-dependent manner.

Genome-wide identification of VDR targets in 1,25(OH)₂D₃-stimulated colonic epithelial cells

To define the transcriptional response to 1,25(OH)₂D₃, we performed sequencing (RNA-seq) of RNA isolated from organoids derived from one healthy individual after 6 and 24 h of stimulation with 1,25(OH)₂D₃ or vehicle treatment. Principal component analysis revealed that the variance was mainly explained by treatment (1,25(OH)₂D₃-treated vs. vehicle) and exposure time (Figure 5A). In total, 283 genes (235 upregulated and 48 downregulated) and 920 genes (567 upregulated and 353 downregulated) were found to be differentially expressed after 6 and 24 h, respectively (thresholds: absolute log₂ fold change (Log₂FC) ≥ 0.5 and false discovery rate (FDR) < 0.05) (Figure 5B, Supplementary Figure S4A–B; Supplementary Table S5). Upregulated genes were related to tight junctions (*CLDN7*), adherens junctions (*CDH1*), Ca²⁺ channels (*TRPV6*), solute transporters (e.g., *SLC2A10* and *SLC30A10*), mucins (*MUC20* and *MUC5B*), the metabolism of various compounds (e.g., *FGF19*, *CYP3A4*, *CYP24A1* and *CYP2B6*), and IEC differentiation (*CA2*), which are all functions related to differentiated cells of the colonic epithelium.^{61–64} Thus, these changes were well aligned with the observed loss of stem cell capacity upon stimulation with 1,25(OH)₂D₃, supporting the assumption that VDR activation mediates this loss.

To investigate 1,25(OH)₂D₃/VDR binding at the chromatin level and for identification of direct VDR target genes, we performed chromatin immunoprecipitation combined with sequencing (ChIP-seq) for VDR using organoids from the same healthy individual used for the RNA-seq analysis. Analysis of VDR binding in two independent experiments following 2 h of stimulation with 1,25(OH)₂D₃ or the vehicle control revealed 253 potential VDR-binding sites, of which 105 were identified in both ChIP-seq replicates (Figure 5C and Supplementary Figure S4C–F). Furthermore, *de novo* motif analysis identified a known consensus DR3-VDRE sequence in 86–94% of the identified peaks (Figure 5D). Annotation of the genes within 10 kb of the identified binding sites revealed 181 potential VDR target genes, which were significantly overrepresented among genes detected as upregulated in the

RNA-seq dataset (Supplementary Figure S4G). Importantly, upon stimulation with $1,25(\text{OH})_2\text{D}_3$, selected genes identified as direct targets (Supplementary Table S6) were upregulated in organoids from both healthy individuals and patients with UC (Figure 5E) in a VDR-dependent manner (Figure 5F). Collectively, these findings supported the conclusion that $1,25(\text{OH})_2\text{D}_3$ exerts a strong effect on IECs via the VDR by promoting transcriptional changes, including the upregulation of a range of differentiation markers and genes involved in intestinal barrier integrity (i.e., tight junctions, adhesion, mucin, etc.).

Expression of direct $1,25(\text{OH})_2\text{D}_3$ target genes is reduced in the inflamed colon in the context of UC

To investigate the expression of the identified vitamin D target genes across patient cohorts, we examined previously published expression data from UC and healthy sigmoid colon biopsies.⁴⁰ Twenty-one genes that we classified as high-confidence upregulated VDR target genes, with a VDR-binding site identified in the two independent CHIP-seq experiments and a greater than twofold change in expression upon $1,25(\text{OH})_2\text{D}_3$ stimulation in the RNA-seq dataset, were analyzed across these cohorts. Among these, the expression levels of 15 genes showed an inverse correlation with disease activity, as assessed by the Mayo score,⁴² with lower expression in inflamed biopsy specimens (Figure 6A–C). The expression levels of CYP24A1, DTNB and TRPV6 showed no correlation with disease activity, while TIMP2 and UCA1 were found to be expressed at higher levels in inflamed biopsy specimens (Supplementary Figure S5). Thus, the reduced VDR levels in the patient cohort correlated with disease severity (Figure 1A-B) and were paralleled by reduced expression of the majority of the 21 identified high-confidence VDR target genes, supporting the applicability of our findings in a clinical setting.

A transcriptional response to 1,25(OH)₂D₃ occurs in crypt-top cell populations

To further explore the effects of 1,25(OH)₂D₃/VDR signaling on colonic epithelial cells, we probed differentially expressed genes from our RNA-seq dataset of 1,25(OH)₂D₃ stimulated organoids against our scRNA-seq datasets. Interestingly, in agreement with the observation that 1,25(OH)₂D₃ exposure increases the expression levels of genes involved in differentiation, both the full list of genes upregulated by 1,25(OH)₂D₃ and the list of 21 direct target genes revealed high expression specifically in fully differentiated colonocytes, BEST4⁺ colonocytes, and goblet cells associated with the top of the crypts (Figure 7A). Moreover, the proportion of cells with high expression of the genes upregulated by 1,25(OH)₂D₃ treatment was significantly lower in the samples from patients with UC than in the samples from healthy individuals (Figure 7B and C) which might be due to a specific loss of the crypt-top population, where VDR normally exerts its activity. Nonetheless, expression of these genes was restricted to cells assigned to the crypt-top domains. These data further show that the 1,25(OH)₂D₃-mediated response is associated with terminally differentiated cells facing the intestinal lumen at the top of the crypts and that 1,25(OH)₂D₃/VDR signaling is impaired in patients with active UC.

Discussion

Although subnormal serum levels of vitamin D are associated with a more aggravated clinical course of UC,^{13,14} the mechanism on how vitamin D affects the human colonic epithelium has remained unknown.

In this study, which complements previous studies of VDR in experimental mouse models^{30,32,33,36,65} and organoids⁶⁶⁻⁶⁸, we performed a detailed analysis of vitamin D–VDR signaling in human colonic epithelial cells. We demonstrated a prominent effect of vitamin D in supporting differentiated cells, mediated directly by VDR. A comprehensive investigation using transcriptional analysis, ChIP-seq, and single-cell sequencing illustrate that vitamin D exposure in vitro induces changes consistent with more differentiated cellular phenotypes that are associated specifically with the epithelial cells

constituting the barrier to the colonic lumen. We suggest that the observed correlation between VDR levels and UC severity is linked with a specific reduction in the number of these terminally differentiated cell types, and that vitamin D signaling is important for safeguarding the functionality of the epithelial barrier.

Based on our experiments using in vitro organoid models, we here demonstrated that activation of vitamin D/VDR signaling attenuates the stem cell potential of colonic epithelial cells, irrespective of whether the cells were isolated from patients with UC or healthy individuals. Importantly, in the VDR KO experiment, we showed that these changes were dependent on VDR expression. A role for vitamin D signaling in the regulation of intestinal stem cell functions has previously been described, involving regulation of genes related to stemness, proliferation and differentiation^{66,68} as well as endoplasmic reticulum (ER) mediated stress (in mice small intestinal organoids).⁶⁸ To expand upon these findings and to reveal the underlying mechanisms, we subsequently performed RNA sequencing on organoids pretreated with either 1,25(OH)₂D₃ or a vehicle control to elucidate the transcriptional response of VDR activation. Utilizing scRNA sequencing allowed for assessment of the heterogeneity of VDR expression among IECs, and mapping vitamin D regulated gene activation to specific cell types within the colonic epithelium. We observed that 1,25(OH)₂D₃ via VDR activates the transcription programs normally associated with terminally differentiated cells, indicating that 1,25(OH)₂D₃ exposure promotes these cellular identities.⁶⁹⁻⁷¹ Moreover, in contrast to the studies of murine organoids, we did not observe enrichment of Gene Ontology terms related to ER stress (Supplementary Table S7), nor did we detect any changes in the levels of the stem marker LGR5. Considering the functional analysis of organoids and the findings from scRNAseq analyses, these observations combined suggest that the effects of VDR signaling are mainly to promote the differentiated cell state rather than active blockade of stem cells.

Terminally differentiated epithelial cells line the colonic lumen and are important for optimal barrier function since they are necessary for proper tight junction formation, mucus secretion, etc.⁷² Various

aspects of intestinal barrier function are regulated by VDR signaling,^{25,38} and VDR protects intestinal barrier permeability in mice.^{30,73} Firstly, tight junctions are regulated by several proteins, including ZO-1, occludin, and E-cadherin.^{73,74} In patients with UC, low serum 25(OH)D levels are associated with decreased levels of ZO-1, occludin, and E-cadherin.⁷⁵ Secondly, VDR signaling, activated by the secondary bile acid, lithocholic acid (LCA), produced by intestinal bacteria, mitigates TNF- α -induced reduction in tight junction proteins and intestinal barrier permeability.⁷⁶ Thirdly, claudin-1, -2, -4, and -7, crucial for tight junction pore regulation, exhibit altered protein levels in patients with UC, which are restored by 1,25(OH)₂D₃ stimulation.^{74,77,78} Thus, a plethora of components are affected by VDR activation and implicated in the barrier integrity.

In line with these previous findings, we report that VDR signaling regulates the expression of genes related to tight junctions, cell adhesion and barrier functions such as claudins, E-cadherin and mucins. As VDR is crucial for maintaining intestinal barrier function and preventing luminal antigen invasion,³⁸ a lack of active vitamin D/VDR signaling in the colonic epithelial barrier may in this way compromise its integrity due to a decreased number and function of differentiated cells; this may cause patients with low serum vitamin D levels to be more susceptible to breach of this barrier, which may in turn cause flares of UC, including ulcerations.³⁸ Data from epidemiological studies have indicated that low serum levels of vitamin D is a risk factor for disease activity of UC.^{17,79,80} Thus, our findings may add to reveal possible mechanisms underlying this observation.

To further validate our findings in relation to UC disease activity, we investigated VDR expression in the colonic epithelial layer in biopsy specimens from patients with UC and healthy individuals by using scRNA-seq and immunohistochemistry. In accordance with previous studies,^{28,32,34,75,81} we found VDR expression to be significantly lower in colonic biopsies from patients with active UC only. We also showed that VDR was expressed at higher levels in the crypt-top cells than in the crypt-bottom population.²⁸ Furthermore, the scRNA-seq data indicated a decreased proportion of fully differentiated cells at the crypt-top in the biopsy samples from inflamed colons. This establishes that

VDR mediates the differentiation of stem cells in the organoid model and primarily exerts its effects at the colonic crypt-top in differentiated epithelial cells. Moreover, VDR expression was found to be lower in patients with active UC than in healthy controls, validating our finding that VDR signaling plays a pivotal role in UC pathogenesis. Additionally, our data suggest colonic VDR expression as a potential biomarker of UC since it correlates well with inflammation and disease severity.^{28,32,81}

Recent reports have linked vitamin D signaling to factors important for the pathogenesis of UC, including immune regulation, intestinal homeostasis and gut barrier function^{23,38}; and as recently uncovered by other research groups, VDR might exert anti-inflammatory actions via the VDR-NLRP6 signaling pathway.⁸²

Here, we have taken a step towards elucidating this matter through experiments in colonic biopsy specimens and human derived organoids. While a potential causal role of VDR signaling during disease development and UC flares cannot be fully explored in this model, we have shown a pivotal role of VDR signaling in supporting differentiation of the human colonic epithelium. Further, the potential for investigation of VDR as a clinical target or biomarker for UC management has been illuminated. It is important to note, that VDR signaling in vivo is mainly mediated by 1,25(OH)₂D₃ binding, and that maintaining sufficient serum levels of 25(OH)D is necessary for proper VDR activity as well as ensuring both skeletal and extra-skeletal health. It is tempting to speculate whether known VDR agonists, such as secondary bile acids like LCA,⁸³ might also play a role in this type of signaling, given our observation that cells adjacent to the intestinal lumen display the highest level of VDR target genes.⁶⁵ Thus, it has been shown that secondary bile acid deficiency may promote intestinal inflammation.⁸⁴ Nonetheless, future clinical trials with non-calcemic VDR agonists, in the efforts to fortify the colonic epithelium, are needed in UC to further clarify the functional role of VDR signaling in human colonic tissue at the molecular level.

Manuscript Doi: 10.1093/ecco-jcc/jjae074

Overall, our data support the hypothesis that VDR signaling plays an important functional role in maintaining human colonic barrier function by regulating cellular differentiation in the colonic intestinal crypts.⁸⁵ Thus, we propose a potential mechanism underlying the correlation of lower vitamin D levels with a more severe disease state in UC through impaired VDR signaling leading to diminished differentiation of the stem cells in the colonic epithelium. This impairment of the vitamin D–VDR axis causes loss of differentiation of the colonic epithelial cells triggering a compromised structure of the colonic epithelial barrier, thereby establishing a pre-inflammatory state and potentially leading to subsequent ulcerations of the colon, a hallmark of flaring UC. By showing the importance of VDR, we also highlight the vitamin D–VDR axis and its regulatory entities as a potential novel target for efforts to explore new therapeutic routes relevant for the management of patients with UC. In this way, our data reveal a novel role of vitamin D signaling in supporting differentiation of the colonic epithelium and take a step toward better understanding the pathophysiology of UC.

Accepted Manuscript

Funding

This work was supported by grants from the Aase and Ejnar Danielsen Foundation (20-10-0353), the Dagmar Marshall Foundation (03-08-2021), the Aage and Johanne Louis-Hansen Foundation (20-2B-8214), the A.P. Moeller Foundation (20-L-0131), the Henrik Henriksen Foundation (28-10-2020), and the Beckett Foundation (20-2-6486) all to LK. This work was further supported by the Memorial Foundation of Solveig Høymann Jacobsen (930-0499 to OHN), the Independent Research Fund Denmark (0134-00111B to KBJ), the Novo Nordisk Foundation (NNF20OC0064376 to KBJ), and the European Union's Horizon 2020 research and innovation program (STEMHEALTH ERCCoG682665 to KBJ). AMB was supported by the Danish Diabetes Academy, which is funded by the Novo Nordisk Foundation (NNF17SA0031406). RBB was supported by fellowships from EMBO (ALTE 946-2019) and MSCA (1183571001/H2020 MSCA). JT was supported by a PhD fellowship from the EU Horizon 2020 Marie Skłodowska-Curie (801481). The Novo Nordisk Foundation Center for Stem Cell Medicine is supported by the Novo Nordisk Foundation (NNF21CC0073729). The funding sources played no role in the study design; the collection, analysis, or interpretation of the data; or the writing of the manuscript.

Acknowledgments

We thank the staff of the Department of Pathology and the Endoscopy Unit, Department of Gastroenterology, Herlev Hospital, for their assistance with handling the patient tissue samples. We also thank the members of the Nielsen and Jensen labs for technical support. We further thank Héctor G. Palmer for providing tissue slides from back skin of wild-type and *Vdr* KO mice. The graphical abstract was created with BioRender.com.

Conflicts of interest

The authors declare no conflicts of interest.

Author contributions

LK, OHN, and KBJ conceptualized the study. LK, LBR, and CS collected patient samples. LK, SLH, JMT, AMB, RBB, MTP, and CS conducted the experiments. GM and JVJ performed the bioinformatic analysis. LK analyzed the data and wrote the first draft of the manuscript with critical input from AG, AH, OHN and KBJ. All authors have critically reviewed and approved the final version of the manuscript.

Ethics

This study was approved by the Scientific Ethics Committee of the Capital Region of Denmark (reg. no. H-18005342). All individuals were informed both orally and in writing, in compliance with the Declaration of Helsinki and the guidelines of the Danish National Scientific Ethics Committee. Written informed consent was obtained prior to inclusion.

Data and material availability

RNA arrays of colonic biopsy samples from patients with ulcerative colitis (UC) and healthy individuals were deposited in the NCBI GEO database (<https://www.ncbi.nlm.nih.gov/geo/query/acc.cgi?acc=GSE206171>). RNA-seq and ChIP-seq data from 1,25(OH)₂D₃-stimulated colonic organoids were deposited in the NCBI GEO database (<https://www.ncbi.nlm.nih.gov/geo/query/acc.cgi?acc=GSE206228>). Single-cell RNA-seq data generated for this paper have been deposited at the European Genome-phenome Archive (EGA) repository and are publicly available as of the date of publication under the accession number EGAS00001007098.

REFERENCES

1. GBD 2017 Inflammatory Bowel Disease Collaborators. The global, regional, and national burden of inflammatory bowel disease in 195 countries and territories, 1990-2017: a systematic analysis for the Global Burden of Disease Study 2017. *Lancet Gastroenterol Hepatol.* 2020;5:17-30.
2. Kaplan GG, Windsor JW. The four epidemiological stages in the global evolution of inflammatory bowel disease. *Nat Rev Gastroenterol Hepatol.* 2021;18:56-66.
3. Wang R, Li Z, Liu S, et al. Global, regional and national burden of inflammatory bowel disease in 204 countries and territories from 1990 to 2019: a systematic analysis based on the Global Burden of Disease Study 2019. *BMJ Open.* 2023;13:e065186.
4. Armuzzi A, Tarallo M, Lucas J, et al. The association between disease activity and patient-reported outcomes in patients with moderate-to-severe ulcerative colitis in the United States and Europe. *BMC Gastroenterol.* 2020;20:18.
5. Le Berre C, Honap S, Peyrin-Biroulet L. Ulcerative colitis. *Lancet.* 2023;402:571-84.
6. Chang JT. Pathophysiology of inflammatory bowel diseases. *N Engl J Med.* 2020;383:2652-64.
7. Zhao M, Gonczi L, Lakatos PL, et al. The burden of inflammatory bowel disease in Europe in 2020. *J Crohns Colitis.* 2021;15:1573-87.
8. Pietschner R, Rath T, Neurath MF, et al. Current and emerging targeted therapies for ulcerative colitis. *Visc Med.* 2023;39:46-53.
9. Hammerhoj A, Boye TL, Langholz E, et al. Mirikizumab (Omvoh) for ulcerative colitis. *Trends Pharmacol Sci.* 2024;45: 281-282.
10. Nielsen OH, Boye TL, Gubatan J, et al. Selective JAK1 inhibitors for the treatment of inflammatory bowel disease. *Pharmacol Ther.* 2023;245:108402.
11. Hausmann A, Steenholdt C, Nielsen OH, et al. Immune cell-derived signals governing epithelial phenotypes in homeostasis and inflammation. *Trends Mol Med.* 2024;30:239-51.
12. Schutgens F, Clevers H. Human organoids: Tools for understanding biology and treating diseases. *Annu Rev Pathol.* 2020;15:211-34.
13. Ananthakrishnan AN. Vitamin D and inflammatory bowel disease. *Gastroenterol Hepatol (N Y).* 2016;12:513-5.
14. Nielsen OH, Rejnmark L, Moss AC. Role of Vitamin D in the Natural History of Inflammatory Bowel Disease. *J Crohns Colitis.* 2018;12:742-52.
15. Liu C, Liu X, Shi H, et al. The correlation between serum 25-hydroxyvitamin D level and ulcerative colitis: a systematic review and meta-analysis. *Eur J Gastroenterol Hepatol.* 2023;35:1375-81.
16. Gubatan J, Chou ND, Nielsen OH, et al. Systematic review with meta-analysis: association of vitamin D status with clinical outcomes in adult patients with inflammatory bowel disease. *Aliment Pharmacol Ther.* 2019;50:1146-58.
17. Gubatan J, Mitsuhashi S, Zenlea T, et al. Low serum vitamin D during remission increases risk of clinical relapse in patients with ulcerative colitis. *Clin Gastroenterol Hepatol.* 2017;15:240-6.
18. Gubatan J, Rubin SJS, Bai L, et al. Vitamin D Is associated with alpha4beta7+ immunophenotypes and predicts vedolizumab therapy failure in patients with inflammatory bowel disease. *J Crohns Colitis.* 2021;15:1980-90.

19. Li XX, Liu Y, Luo J, et al. Vitamin D deficiency associated with Crohn's disease and ulcerative colitis: a meta-analysis of 55 observational studies. *J Transl Med.* 2019;17:323.
20. Ulitsky A, Ananthakrishnan AN, Naik A, et al. Vitamin D deficiency in patients with inflammatory bowel disease: association with disease activity and quality of life. *JPEN J Parenter Enteral Nutr.* 2011;35:308-16.
21. Nielsen OH, Hansen TI, Gubatan JM, et al. Managing vitamin D deficiency in inflammatory bowel disease. *Frontline Gastroenterol.* 2019;10:394-400.
22. Bilezikian JP, Formenti AM, Adler RA, et al. Vitamin D: Dosing, levels, form, and route of administration: Does one approach fit all? *Rev Endocr Metab Disord.* 2021;22:1201-18.
23. Triantos C, Aggeletopoulou I, Mantzaris GJ, et al. Molecular basis of vitamin D action in inflammatory bowel disease. *Autoimmun Rev.* 2022;21:103136.
24. Wallace C, Gordon M, Sinopoulou V, et al. Vitamin D for the treatment of inflammatory bowel disease. *Cochrane Database Syst Rev.* 2023;10:CD011806.
25. Kellermann L, Jensen KB, Bergenheim F, et al. Mucosal vitamin D signaling in inflammatory bowel disease. *Autoimmun Rev.* 2020;19:102672.
26. Barbachano A, Fernandez-Barral A, Ferrer-Mayorga G, et al. The endocrine vitamin D system in the gut. *Mol Cell Endocrinol.* 2017;453:79-87.
27. Carlberg C. Vitamin D and its target genes. *Nutrients.* 2022;14:1354.
28. Garg M, Royce SG, Tikellis C, et al. The intestinal vitamin D receptor in inflammatory bowel disease: inverse correlation with inflammation but no relationship with circulating vitamin D status. *Therap Adv Gastroenterol.* 2019;12:1756284818822566.
29. Aggeletopoulou I, Marangos M, Assimakopoulos SF, et al. Vitamin D and microbiome: Molecular interaction in inflammatory bowel disease pathogenesis. *Am J Pathol.* 2023;193:656-68.
30. Guo Y, Li X, Geng C, et al. Vitamin D receptor involves in the protection of intestinal epithelial barrier function via up-regulating SLC26A3. *J Steroid Biochem Mol Biol.* 2023;227:106231.
31. Kosinsky RL, Zerche M, Kutschat AP, et al. RNF20 and RNF40 regulate vitamin D receptor-dependent signaling in inflammatory bowel disease. *Cell Death Differ.* 2021;28:3161-75.
32. Liu W, Chen Y, Golan MA, et al. Intestinal epithelial vitamin D receptor signaling inhibits experimental colitis. *J Clin Invest.* 2013;123:3983-96.
33. Lu R, Zhang YG, Xia Y, et al. Imbalance of autophagy and apoptosis in intestinal epithelium lacking the vitamin D receptor. *FASEB J.* 2019;33:11845-56.
34. Lu R, Zhang YG, Xia Y, et al. Paneth cell alertness to pathogens maintained by vitamin D receptors. *Gastroenterology.* 2021;160:1269-83.
35. Waterhouse M, Hope B, Krause L, et al. Vitamin D and the gut microbiome: a systematic review of in vivo studies. *Eur J Nutr.* 2019;58:2895-910.
36. Wu S, Zhang YG, Lu R, et al. Intestinal epithelial vitamin D receptor deletion leads to defective autophagy in colitis. *Gut.* 2015;64:1082-94.
37. Zhang Y, Garrett S, Carroll RE, et al. Vitamin D receptor upregulates tight junction protein claudin-5 against colitis-associated tumorigenesis. *Mucosal Immunol.* 2022;15:683-97.

38. Sun J, Zhang YG. Vitamin D receptor influences intestinal barriers in health and disease. *Cells*. 2022;11:1129.
39. Soendergaard C, Kvist PH, Seidelin JB, et al. Systemic and intestinal levels of factor XIII-A: the impact of inflammation on expression in macrophage subtypes. *J Gastroenterol*. 2016;51:796-807.
40. Soendergaard C, Kvist PH, Thygesen P, et al. Characterization of growth hormone resistance in experimental and ulcerative colitis. *Int J Mol Sci*. 2017;18:2046.
41. Soendergaard C, Nielsen OH, Seidelin JB, et al. Alpha-1 antitrypsin and granulocyte colony-stimulating factor as serum biomarkers of disease severity in ulcerative colitis. *Inflamm Bowel Dis*. 2015;21:1077-88.
42. Schroeder KW, Tremaine WJ, Ilstrup DM. Coated oral 5-aminosalicylic acid therapy for mildly to moderately active ulcerative colitis. A randomized study. *N Engl J Med*. 1987;317:1625-9.
43. Maciag G, Hansen SL, Krizic K, et al. JAK/STAT signaling promotes the emergence of unique cell states in ulcerative colitis. *bioRxiv*. 2024; <https://doi.org/10.1101/2024.01.22.576736>.
44. Sato T, Stange DE, Ferrante M, et al. Long-term expansion of epithelial organoids from human colon, adenoma, adenocarcinoma, and Barrett's epithelium. *Gastroenterology*. 2011;141:1762-72.
45. Bergenheim F, Fregni G, Buchanan CF, et al. A fully defined 3D matrix for ex vivo expansion of human colonic organoids from biopsy tissue. *Biomaterials*. 2020;262:120248.
46. Geboes K, Riddell R, Ost A, et al. A reproducible grading scale for histological assessment of inflammation in ulcerative colitis. *Gut*. 2000;47:404-9.
47. Andrews S. FastQC. A quality control tool for high throughput sequence data. 2019 [Available from: <https://www.bioinformatics.babraham.ac.uk/projects/fastqc/>].
48. Wingett S. FastQ Screen allows you to screen a library of sequences in FastQ format against a set of sequence databases so you can see if the composition of the library matches with what you expect. 2019 [Available from: https://www.bioinformatics.babraham.ac.uk/projects/fastq_screen/].
49. Chen S, Zhou Y, Chen Y, et al. fastp: an ultra-fast all-in-one FASTQ preprocessor. *Bioinformatics*. 2018;34:i884-i90.
50. Dobin A, Davis CA, Schlesinger F, et al. STAR: ultrafast universal RNA-seq aligner. *Bioinformatics*. 2013;29:15-21.
51. Liao Y, Smyth GK, Shi W. featureCounts: an efficient general purpose program for assigning sequence reads to genomic features. *Bioinformatics*. 2014;30:923-30.
52. Love MI, Huber W, Anders S. Moderated estimation of fold change and dispersion for RNA-seq data with DESeq2. *Genome Biol*. 2014;15:550.
53. Langmead B, Trapnell C, Pop M, et al. Ultrafast and memory-efficient alignment of short DNA sequences to the human genome. *Genome Biol*. 2009;10:R25.
54. Kharchenko PV, Tolstorukov MY, Park PJ. Design and analysis of ChIP-seq experiments for DNA-binding proteins. *Nat Biotechnol*. 2008;26:1351-9.
55. Zhang Y, Liu T, Meyer CA, et al. Model-based analysis of ChIP-Seq (MACS). *Genome Biol*. 2008;9:R137.

56. Ma W, Noble WS, Bailey TL. Motif-based analysis of large nucleotide data sets using MEME-ChIP. *Nat Protoc.* 2014;9:1428-50.
57. Wang L, Wang S, Li W. RSeQC: quality control of RNA-seq experiments. *Bioinformatics.* 2012;28:2184-5.
58. Fujii M, Matano M, Nanki K, et al. Efficient genetic engineering of human intestinal organoids using electroporation. *Nat Protoc.* 2015;10:1474-85.
59. Conant D, Hsiao T, Rossi N, et al. Inference of CRISPR edits from Sanger trace data. *CRISPR J.* 2022;5:123-30.
60. Arnauts K, Verstockt B, Ramalho AS, et al. Ex vivo mimicking of inflammation in organoids derived from patients with ulcerative colitis. *Gastroenterology.* 2020;159:1564-7.
61. Bekku S, Mochizuki H, Takayama E, et al. Carbonic anhydrase I and II as a differentiation marker of human and rat colonic enterocytes. *Res Exp Med (Berl).* 1998;198:175-85.
62. Janssen AWF, Duivenvoorde LPM, Rijkers D, et al. Cytochrome P450 expression, induction and activity in human induced pluripotent stem cell-derived intestinal organoids and comparison with primary human intestinal epithelial cells and Caco-2 cells. *Arch Toxicol.* 2021;95:907-22.
63. Yamamoto-Furusho JK, Ascano-Gutierrez I, Furuzawa-Carballeda J, et al. Differential Expression of MUC12, MUC16, and MUC20 in Patients with Active and Remission Ulcerative Colitis. *Mediators Inflamm.* 2015;2015:659018.
64. Chelakkot C, Ghim J, Ryu SH. Mechanisms regulating intestinal barrier integrity and its pathological implications. *Exp Mol Med.* 2018;50:1-9.
65. Reynolds CJ, Koszewski NJ, Horst RL, et al. Localization of the 1,25-dihydroxyvitamin d-mediated response in the intestines of mice. *J Steroid Biochem Mol Biol.* 2019;186:56-60.
66. Fernandez-Barral A, Costales-Carrera A, Buirra SP, et al. Vitamin D differentially regulates colon stem cells in patient-derived normal and tumor organoids. *FEBS J.* 2020;287:53-72.
67. Li J, Witonsky D, Sprague E, et al. Genomic and epigenomic active vitamin D responses in human colonic organoids. *Physiol Genomics.* 2021;53:235-48.
68. Sittipo P, Kim HK, Han J, et al. Vitamin D(3) suppresses intestinal epithelial stemness via ER stress induction in intestinal organoids. *Stem Cell Res Ther.* 2021;12:285.
69. Bakke DS, Zhang J, Zhang Y, et al. Myeloid vitamin D receptor regulates Paneth cells and microbial homeostasis. *FASEB J.* 2023;37:e22957.
70. Lin Y, Xia P, Cao F, et al. Protective effects of activated vitamin D receptor on radiation-induced intestinal injury. *J Cell Mol Med.* 2023;27:246-58.
71. Treveil A, Sudhakar P, Matthews ZJ, et al. Regulatory network analysis of Paneth cell and goblet cell enriched gut organoids using transcriptomics approaches. *Mol Omics.* 2020;16:39-58.
72. Capaldo CT, Powell DN, Kalman D. Layered defense: how mucus and tight junctions seal the intestinal barrier. *J Mol Med (Berl).* 2017;95:927-34.
73. Kong J, Zhang Z, Musch MW, et al. Novel role of the vitamin D receptor in maintaining the integrity of the intestinal mucosal barrier. *Am J Physiol Gastrointest Liver Physiol.* 2008;294:G208-16.
74. Lee C, Lau E, Chusilp S, et al. Protective effects of vitamin D against injury in intestinal epithelium. *Pediatr Surg Int.* 2019;35:1395-401.

75. Meckel K, Li YC, Lim J, et al. Serum 25-hydroxyvitamin D concentration is inversely associated with mucosal inflammation in patients with ulcerative colitis. *Am J Clin Nutr.* 2016;104:113-20.
76. Yao B, He J, Yin X, et al. The protective effect of lithocholic acid on the intestinal epithelial barrier is mediated by the vitamin D receptor via a SIRT1/Nrf2 and NF-kappaB dependent mechanism in Caco-2 cells. *Toxicol Lett.* 2019;316:109-18.
77. Stio M, Retico L, Annese V, et al. Vitamin D regulates the tight-junction protein expression in active ulcerative colitis. *Scand J Gastroenterol.* 2016;51:1193-9.
78. Domazetovic V, Iantomasi T, Bonanomi AG, et al. Vitamin D regulates claudin-2 and claudin-4 expression in active ulcerative colitis by p-Stat-6 and Smad-7 signaling. *Int J Colorectal Dis.* 2020;35:1231-42.
79. Guzman-Prado Y, Samson O, Segal JP, et al. Vitamin D therapy in adults with inflammatory bowel disease: A systematic review and meta-analysis. *Inflamm Bowel Dis.* 2020;26:1819-30.
80. Johansen I, Smastuen MC, Lokkeberg ST, et al. Symptoms and symptom clusters in patients newly diagnosed with inflammatory bowel disease: results from the IBSEN III Study. *BMC Gastroenterol.* 2023;23:255.
81. Zhang YG, Lu R, Xia Y, et al. Lack of vitamin D receptor leads to hyperfunction of claudin-2 in intestinal inflammatory responses. *Inflamm Bowel Dis.* 2019;25:97-110.
82. Gao H, Zhou H, Zhang Z, et al. Vitamin D3 alleviates inflammation in ulcerative colitis by activating the VDR-NLRP6 signaling pathway. *Front Immunol.* 2023;14:1135930.
83. Sasaki H, Masuno H, Kawasaki H, et al. Lithocholic acid derivatives as potent vitamin D receptor agonists. *J Med Chem.* 2021;64:516-26.
84. Sinha SR, Haileselassie Y, Nguyen LP, et al. Dysbiosis-induced secondary bile acid deficiency promotes intestinal inflammation. *Cell Host Microbe.* 2020;27:659-70 e5.
85. Fleet JC. Vitamin D and Gut Health. *Adv Exp Med Biol.* 2022;1390:155-67.

ACCEPTED MANUSCRIPT

Figure legends

Fig. 1. Colonic VDR expression is reduced in patients with active ulcerative colitis (UC).

- (A) Plot of VDR expression in healthy participants and UC patients. VDR expression was assessed via RNA array in sigmoid colon biopsy specimens from healthy individuals (n = 19) and patients with UC (n = 59), who were grouped according to disease activity based on the Mayo score. Y-axis: log of normalized gene expression levels. Data are presented as the mean \pm SEM. One-way ANOVA with Tukey's multiple comparison test. *** $P < 0.0001$, ** $P = 0.0017$.
- (B) VDR protein expression was assessed by immunohistochemistry (IHC) intensity scores. A score of 0–3 (negative (0), weak (1), moderate (2), and strong (3)) was assigned to two biopsy specimens from each individual to calculate the mean score. The horizontal line represents the mean values. One-way ANOVA with Tukey's multiple comparison test. *** $P < 0.0001$.
- (C)-(D) A representative IHC image of a VDR-stained colonic biopsy from a healthy individual (C) and a patient with UC with severe disease activity (D). Scale bar = 100 μ m.
- (E) Isotype control stained colonic biopsy from a patient with UC
- (F) Scatterplot of VDR expression vs. the Mayo score. Spearman's correlation test. Black line: linear regression; dotted lines: 95% confidence interval
- (G) Scatterplot of VDR expression vs. the Geboes score. Spearman's correlation test. Black line: linear regression; dotted lines: 95% confidence interval

Fig. 2. Colonic VDR expression is high in the crypt-top domains.

Analysis of single-cell RNA sequencing (scRNA-seq) data of 11 035 colonic epithelial cells from four healthy individuals and 4 354 colonic epithelial cells from four patients with active ulcerative colitis (UC).

- (A) UMAP plot of cell states in the healthy epithelium. TA, transit amplifying; CT, crypt-top; EECs, enteroendocrine cells.
- (B) UMAP plot of *VDR* expression in cells in the healthy epithelium.
- (C) UMAP plot of cells in the inflamed epithelium.
- (D) UMAP plot of *VDR* expression in cells in the inflamed epithelium.
- (E) Top left: normal epithelium from a colonic resection specimen, hematoxylin and eosin (H&E). Top right: normal colonic epithelium, VDR staining. Bottom left: inflamed colonic epithelium, H&E. Bottom right: inflamed colonic epithelium, VDR staining. Scale bar = 250 μm . * = Top of crypts at the epithelial surface. Insert = VDR stained slide overview.
- (F) Percentage of cells identified using the scRNA-seq data as crypt-top cells in samples of healthy tissue and inflamed tissue from UC patients. Error bars represent the SEM. Wilcoxon rank-sum test.

Fig. 3. 1,25(OH)₂D₃ exerts antiproliferative effects and reduces the organoid formation capacity of colonic epithelial cells.

Organoids were stimulated with 100 nM 1,25(OH)₂D₃ or the vehicle control for ten days, corresponding to one passage. On day 10, five representative images of each well were captured. The organoids were derived from six patients with UC and six healthy individuals, and all experiments were performed in triplicate.

- (A) Immunohistochemical staining for VDR in formalin-fixed and paraffin-embedded colonic organoids. Scale bar = 100 μm.
- (B) Images of organoids on day 10 following continuous stimulation with either 1,25(OH)₂D₃ or the vehicle control representative of n=6 participants from each group. Bright-field images (objective: 5x). Scale bar = 200 μm.
- (C) Plot of the individual sizes (μm²) of colonic organoids from six healthy individuals and six patients with UC. Horizontal lines represent the mean. Welch's t test.
- (D) The organoid size and number of organoids per area normalized to those in the corresponding vehicle control group. Horizontal black lines represent the mean. The red dotted line represents vehicle after normalization. The Wilcoxon test was used to compare paired values (**P* = 0.0313 on all plots). The Mann–Whitney U test was used to compare the healthy and UC patient samples. ns, not significant.
- (E) Images captured on day 10 after reseeding the cells from one healthy individual and one patient with UC representative of n=6 participants from each group. Bright-field images (objective: 5x). Scale bar = 200 μm.

(F) Organoid forming capacity. Plot of the number of organoids formed after re-seeding of 1,25(OH)₂D₃-treated organoids normalized to vehicle control levels for healthy participants and UC patients. Wilcoxon test **P* = 0.0313, ns: not significant.

Fig. 4. The effects of 1,25(OH)₂D₃ on proliferation and self-renewal potential are dependent on VDR expression.

CRISPR/Cas9 knockout of *VDR* was performed in organoids from one healthy individual.

- (A) Western blotting and (B) immunohistochemistry showing effective loss of VDR in CRISPR/Cas9-edited organoids compared to those derived from the parental line. Scale bar = 100 μm.
- (C) Bright-field images (objective: 5x) of *VDR*-knockout organoids and the corresponding parental organoids, which were seeded at 7 500 cells per Matrigel droplet and embedded in medium supplemented with either 100 nM 1,25(OH)₂D₃ or the vehicle control. On day 10, five representative images of each well were acquired. Scale bar = 200 μm.
- (D) The organoids were collected and processed into single-cell suspensions. The yield per seeded cell upon 1,25(OH)₂D₃ stimulation normalized to the vehicle control was calculated. The number of organoids per unit area and organoid size were measured using representative images and normalized to the corresponding vehicle control group. The data represent the mean of three replicates.
- (E) Bright-field images (objective: 5x) of organoids after single-cell suspensions were reseeded at 5 000 cells per Matrigel droplet and cultured for 10 days in

Manuscript Doi: 10.1093/ecco-jcc/jjae074
 standard organoid medium. Representative images captured on day 10 after
 reseeding the cells. Scale bar = 200 μ m.

- (F) The number of organoids formed after $1,25(\text{OH})_2\text{D}_3$ treatment was normalized to the number of organoids formed after treatment with the corresponding vehicle control.

Fig. 5. Identification of genome-wide VDR targets in $1,25(\text{OH})_2\text{D}_3$ -stimulated colonic organoids.

Organoids from one healthy individual were treated with $1,25(\text{OH})_2\text{D}_3$ or the vehicle control for 6 and 24 h in triplicate for each time point. The transcriptional response was evaluated using bulk RNA sequencing.

- (A) Principal component (PC) analysis was performed to cluster samples by time and treatment.
- (B) Volcano plot of differentially expressed genes after 24 h of stimulation with $1,25(\text{OH})_2\text{D}_3$; 567 were upregulated, and 353 were downregulated (absolute \log_2 fold change ≥ 0.05 and false discovery rate < 0.05).
- (C) Organoids from the same healthy individual were treated for 2 h with $1,25(\text{OH})_2\text{D}_3$ or the vehicle control. Chromatin interactions were studied by CHIP-seq with two replicates. Integrative Genome Visualization representation of VDR-binding sites identified near the selected VDR target genes.
- (D) *De novo* motif analysis revealed a consensus VDR response DR3 element in 85% and 94% of the identified peaks in two CHIP-seq replicates, respectively.
- (E) Organoids derived from six healthy individuals and six UC patients were stimulated with 1 μ M $1,25(\text{OH})_2\text{D}_3$ for 24 h on day 6. The changes in the expression levels of the selected VDR target genes were evaluated by qPCR. A Wilcoxon test was used to compare paired samples for $1,25(\text{OH})_2\text{D}_3$ vs. the

Manuscript Doi: 10.1093/ecco-jcc/jjae074
 vehicle control. All the genes were significantly upregulated ($P = 0.0313$).

Boxes indicate the range, the lines in boxes indicate the mean, and the dotted line indicates vehicle after normalization.

(F) Gene expression fold change relative to the vehicle control group analyzed by qPCR for selected VDR target genes after 24 h of $1,25(\text{OH})_2\text{D}_3$ stimulation in VDR knockout organoids and matching parental organoids. Data represent the mean of three replicates.

Fig. 6. The expression levels of VDR target genes are reduced in the inflamed colons of UC patients.

The expression levels of the identified VDR target genes were analyzed using RNA array data from sigmoid colon biopsy samples from healthy individuals ($n = 19$) and patients with UC ($n = 59$).

- (A) *SLC30A10* expression grouped by disease activity. Data are shown as the mean \pm SEM. One-way ANOVA with Tukey's multiple comparison test. $***P < 0.0001$, $**P = 0.0029$. *SLC30A10* expression is shown as a representative example. The remaining gene expression plots are included in Supplementary Figure S5.
- (B) Scatterplot of *SLC30A10* expression vs. the Mayo score. Spearman's correlation test.
- (C) Spearman's correlation coefficients for the identified VDR target genes vs. the Mayo score.

Fig. 7. The transcriptional response to 1,25(OH)₂D₃ occurs in VDR-expressing crypt-top epithelial cells.

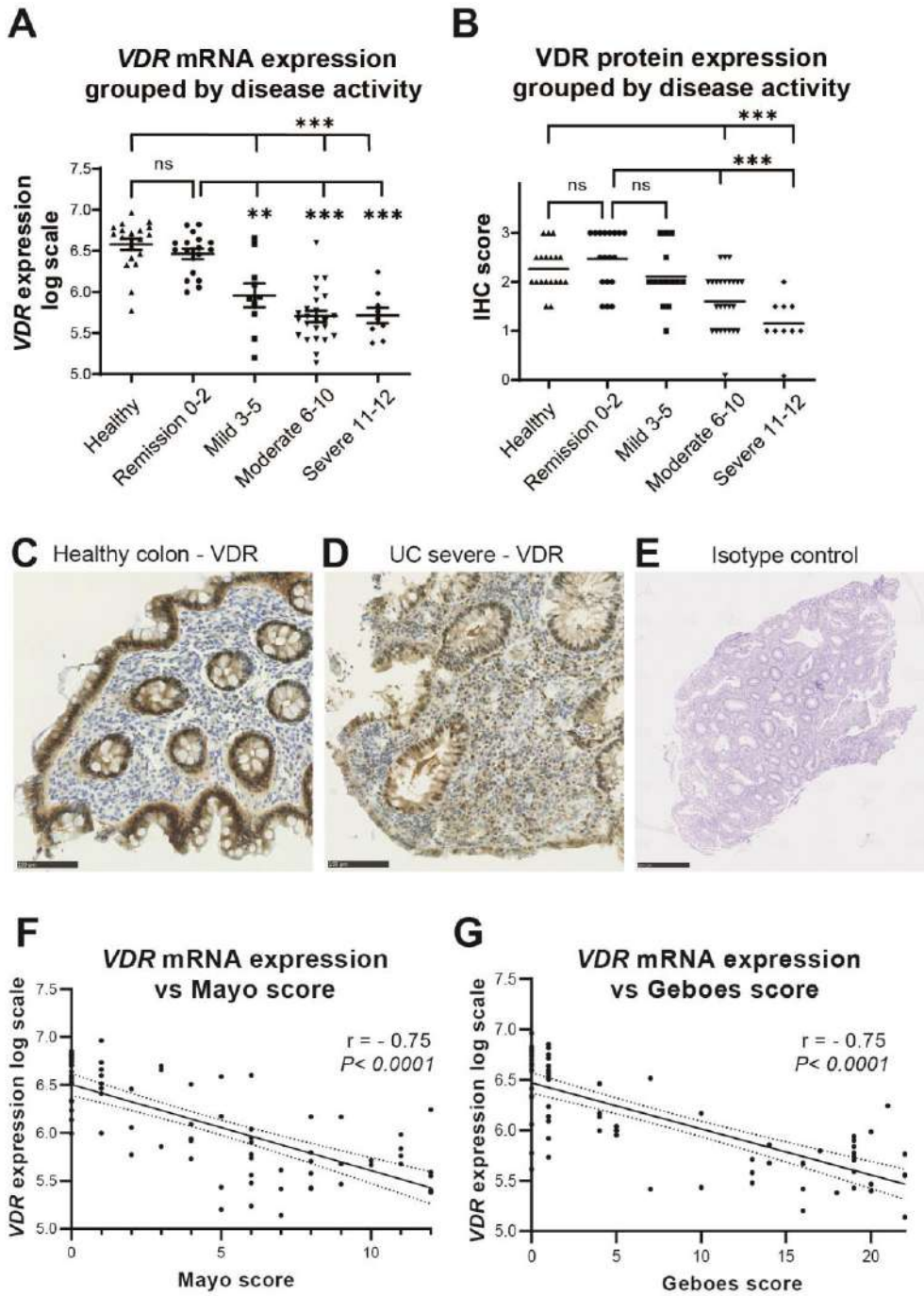
- (A) Single-cell RNA-seq data for the healthy epithelium. Left: UMAP plot of the enrichment of genes that were upregulated upon 1,25(OH)₂D₃ stimulation for 24 h. Right: UMAP plot of the enrichment of 21 VDR target genes.
- (B) Single-cell RNA-seq data for the inflamed epithelium. Left: UMAP plot of the enrichment of genes that were upregulated upon 1,25(OH)₂D₃ stimulation for 24 h. Right: UMAP plot of the enrichment of the 21 VDR target genes.
- (C) Fraction of cells in the scRNA-seq dataset with positive enrichment of genes upregulated upon 1,25(OH)₂D₃ stimulation.

Accepted Manuscript

Table 1

Gene expression vs Mayo score		
Gene	r	P-value
<i>Genes with lower expression in inflamed samples</i>		
CEACAM7	-0.2407	0.0338
GUCA2A	-0.7493	<0.0001
SLC26A3	-0.4757	<0.0001
KRT20	-0.2374	0.0364
MS4A12	-0.389	0.0004
GUCA2B	-0.7479	<0.0001
AQP8	-0.7967	<0.0001
FTH1	-0.716	<0.0001
TMIGD1	-0.7381	<0.0001
HPGD	-0.5226	<0.0001
MUC12	-0.4136	0.0002
CLCA4	-0.2259	0.0468
ABCG2	-0.7675	<0.0001
CA4	-0.3924	0.0004
CFDP1	-0.5654	<0.0001
<i>Genes with higher expression in inflamed samples</i>		
CEACAM6	0.2867	0.0109
<i>No difference between non-inflamed and inflamed</i>		
PLAC8	0.1469	ns
NEAT1	0.004326	ns
IFI27	0.1266	ns
CEACAM1	0.2069	ns

The expression levels of the top 20 crypt-top defining genes from the single-cell RNA sequencing analysis genes were analyzed using the RNA array dataset. Pearson's r correlation of gene expression vs. The Mayo score are shown.



A

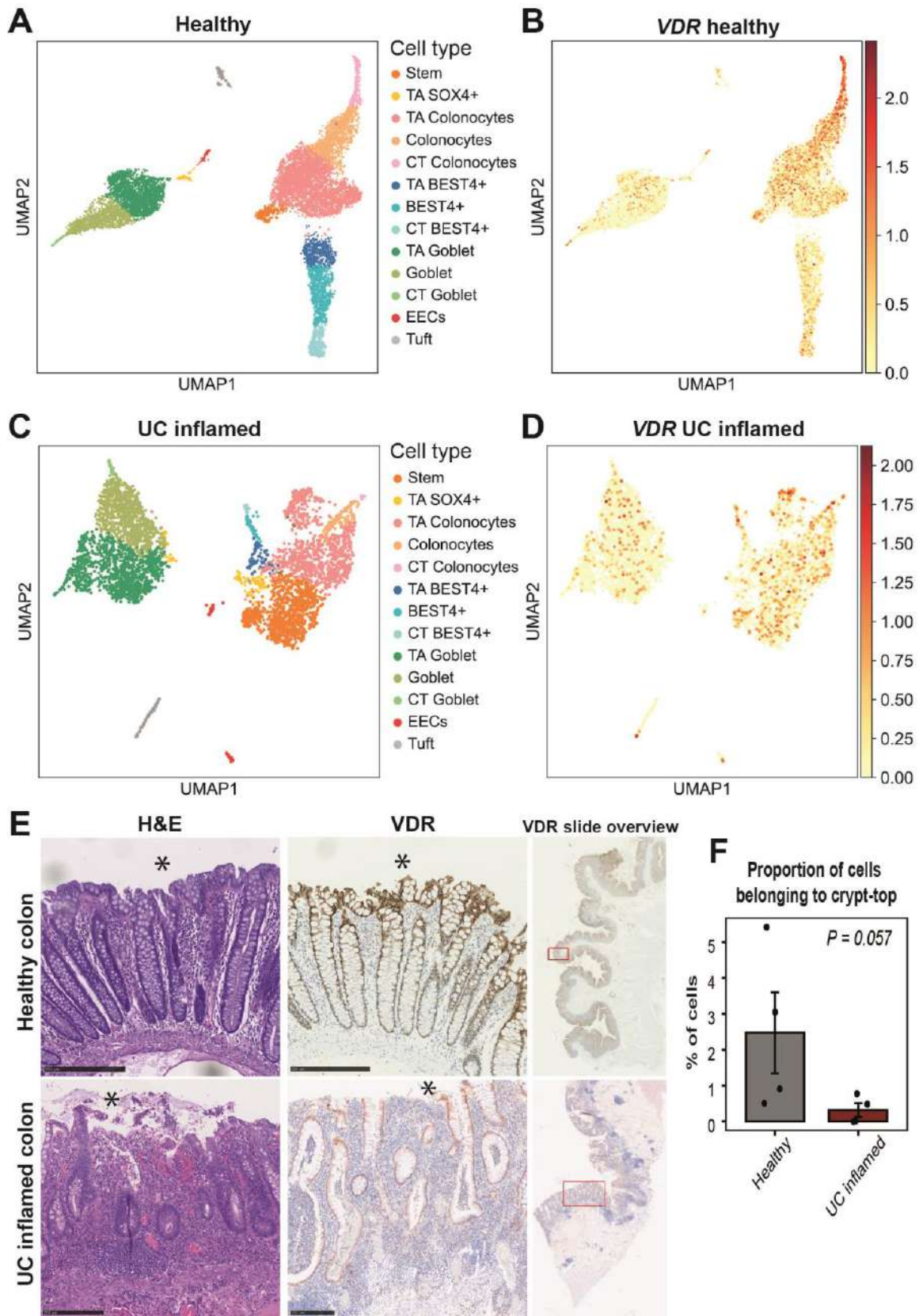
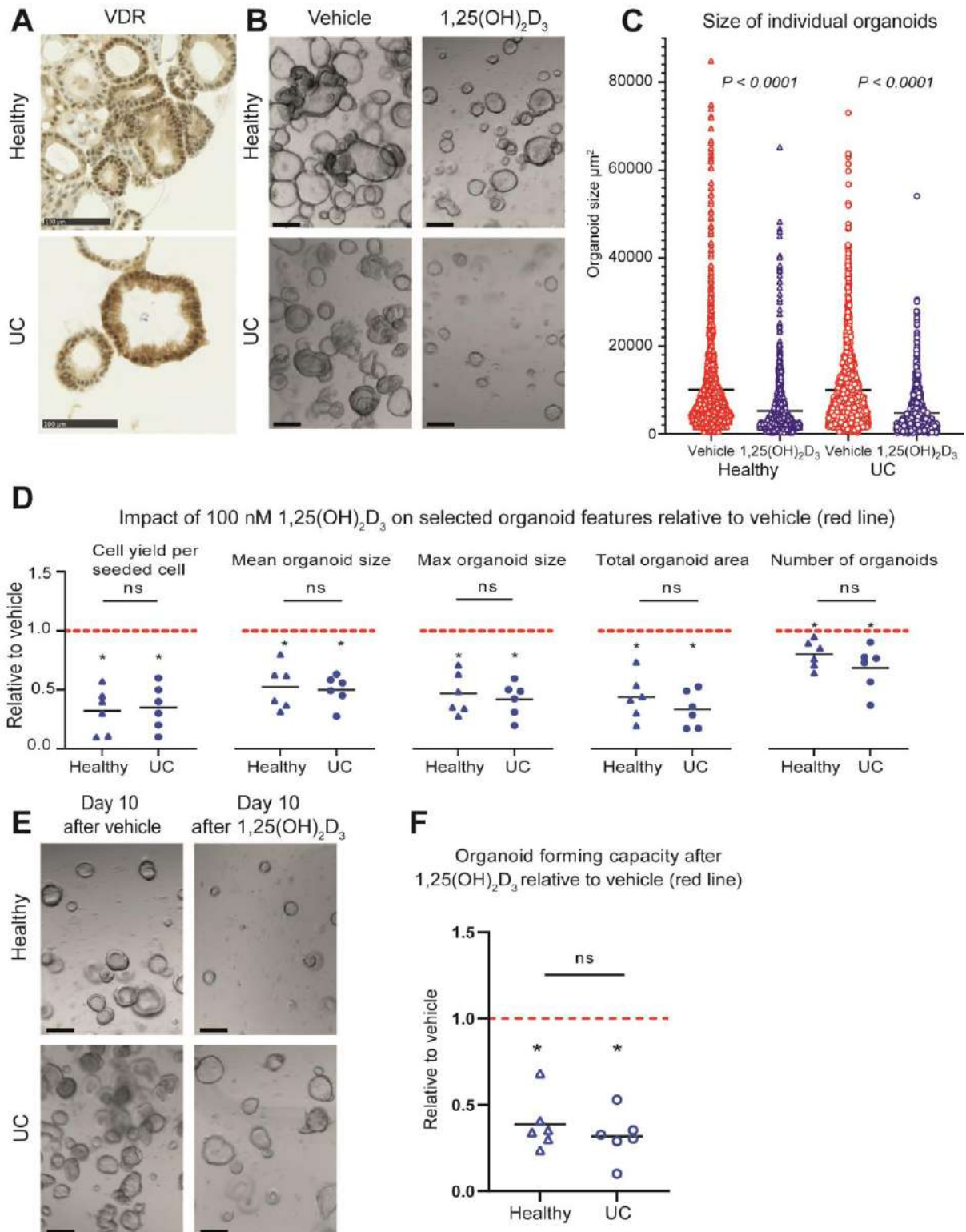
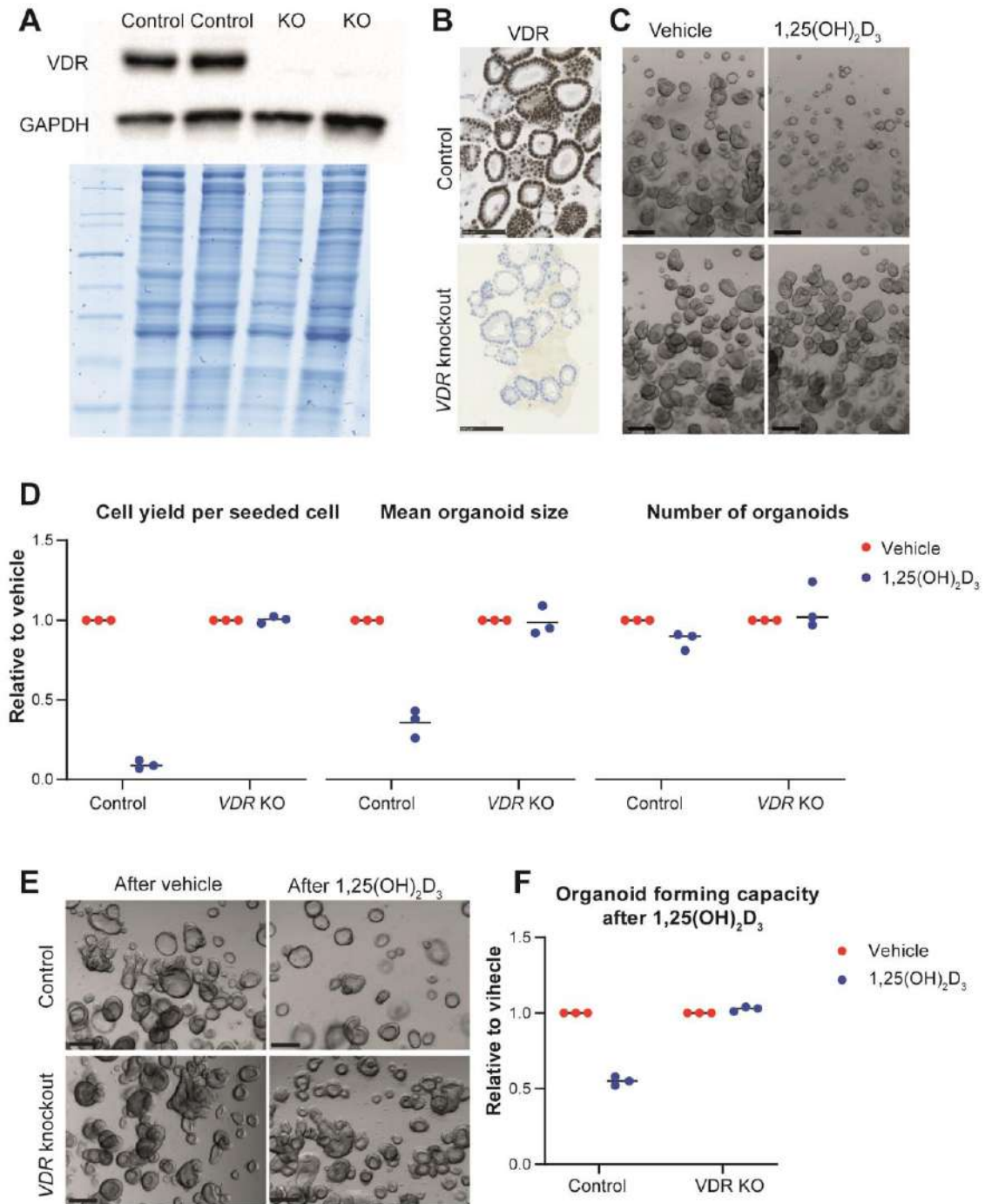
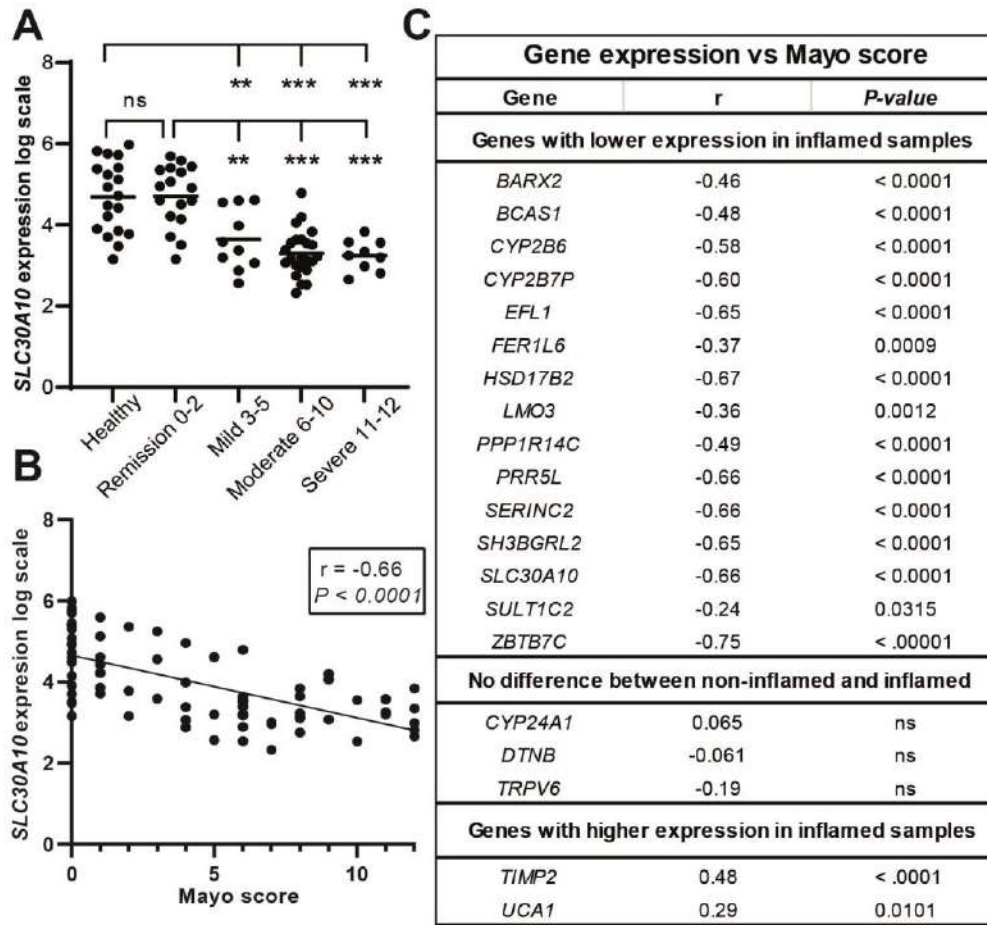


Figure 3



Manuscript Doi: 10.1093/ecco-jcc/jjae074
Figure 4





Accepted

